Title: Reflow transfer for conformal 3-dimensional microprinting

Authors: G. Zabow[1]*

Affiliations:

[1]Applied Physics Division, National Institute of Standards and Technology; Boulder, Colorado, 80305, USA.

*Corresponding author. Email: gary.zabow@nist.gov

Abstract: From microcircuits to metamaterials, micropatterning surfaces adds valuable functionality. For non-planar surfaces, however, incompatibility with conventional microlithography requires transferring originally planar micropatterns onto those surfaces but existing approaches accommodate only limited curvatures. A microtransfer approach is developed using reflowable materials that transform between solid and liquid on demand, freely stretching to yield transfers that naturally conform down to nanoscale radii of curvature and arbitrarily complex topographies. Such reflow transfer helps generalize microprinting, extending the reach of precision planar microlithography to highly non-planar substrates and microstructures. With gentle water-based processing, reflow transfer can be applied to a range of materials, with microprinting demonstrated onto metal, plastic, paper, glass, polystyrene, semiconductor, elastomer, hydrogel, and multiple biological surfaces.

One-Sentence Summary: Regular table sugar enables generalized microprinting onto microstructures and other previously intractable surfaces.

Main Text:

Fueled by the semiconductor industry, microfabrication tools have evolved to pattern ever more precisely and efficiently, but only on rigid, planar surfaces. Leveraging these mature lithographic technologies for advanced manufacturing of soft or non-planar substrates requires transferring initially planar microfabricated designs onto these alternative materials. While research over the past decades has yielded multiple transfer printing techniques (*1, 2*) able to transfer microstructures onto various soft or gently curved substrates common to fields such as flexible electronics and biointegrated sensing (*3*), accurate transfer onto more general surfaces of arbitrary curvature has remained elusive (*2, 4*).

All transfer microprinting methods currently transport micropatterns or structures between substrates via either a solid or liquid transfer medium, or carrier. Solid carriers, commonly based on elastomers (*5*) or adhesive tapes (*6*), facilitate accurate placement and robust macroscopic handling of microscopic structures. However, even flexible solid carriers can deform only so far, impeding conformal transfer onto high curvature substrates or microstructures. Additionally, contact pressures needed to lift microstructures from their original substrates or to conform to receiving substrates, can limit transfer of fragile structures or onto fragile substrates. Alternatively, liquids can gently float microstructures between substrates, improving conformability by supporting thinner, more flexible, carriers (*7*) or by employing the liquid itself as the carrier *(8*). However, wet transfers sacrifice placement accuracy and incur buoyancy and hydrophobicity limitations.

Here, a printing process is described using thermally reflowable carriers that can controllably, and locally, transform between solid and liquid on demand. Combining advantages of both wet and dry transfer, the process overcomes drawbacks of each, enabling accurately positioned, ultra-conformal printing over a wide array of surfaces, including those too topographically challenging to be patterned by other methods. This REflow-driven FLExible Xfer (REFLEX) process is introduced using an unlikely material from a microfabrication viewpoint: regular table sugar (sucrose). Sugar is often dismissed because it crystallizes, yielding inhomogeneous surfaces incompatible with microfabrication (*9*). However, as known in food processing, adding corn syrup prevents crystallization and caramelized sugar and corn syrup mixtures need not disturb micropattern geometries. Sugar mixtures also offer favorable low glass transition temperatures, T_g, near room temperature that are tailorable based on composition (*10*) and degree of caramelization (*11*). Moreover, sugar mixtures fully dissolve in water further broadening substrate compatibility by eliminating any carrier adhesion complications and enabling clean, physically and chemically gentle transfers free of any high temperatures, harsh solvents, or aggressive etchings needed to remove other common transfer intermediates or residues (*2*).

One simple composition comprises sugar and corn syrup heated with water until caramelized (*12*). Once cooled, the resulting solid can be melted or redissolved in water for pouring over micropatterns or structures that are to be transferred, with any remaining water subsequently removed via evaporative heating (Fig. 1A and fig. S1). Depending on substrate materials, the resulting sugar coating can be delaminated directly or released by dissolving an underlying sacrificial layer: while water soluble, sugar resists dissolution in common solvents like acetone allowing selective release with widely available photoresists or other acetone-soluble materials (12). Being optically transparent, the released sugar layer with the transfer microstructures partially embedded in its underside can then be accurately positioned, with micrometer level precision (fig. S2), on the receiving substrate and softened by gentle heating. The resulting

viscous, creeping fluid carries with it the microstructures, ultra-conformally coating them over the receiving substrate before the sugar is finally dissolved away. Because the fluid can conform to the shape of its container (or underlying surface), the surface curvature or feature sharpness that can be patterned is in principle unlimited. Meanwhile, unlike free-flowing liquids, the high reflow viscosity helps maintain the relative positions of structures during transfer, largely suppressing disturbing liquid currents, translational forces between free-floating structures, and surface tension driven dislocations, which frustrate traditional wet transfer enough to necessitate special-purpose floating microrobot aligners (*13*, *14*).

As a first example of a simple substrate that is hard to pattern by any other technique, Fig. 1B shows an array of microfabricated disks, which double as microscale fiducial markers, transferred onto a surface with recessed holes. REFLEX microprinting patterns the whole surface, including down vertical sidewalls and over edges with nanoscale radii of curvature, for both rigid and flexible microstructures (fig. S3). Altered array spacings map the transfer material reflow as it locally stretches to cover new surfaces, which may differ in area from those on which the arrays were originally fabricated. For example, the extra sidewall forming the hole shown in Fig. 1B, triples the local area to be accommodated. Such stretching would confound existing solid-based transfer schemes while surface tension effects at the abrupt feature edges would also disrupt liquid-based approaches (*14*); REFLEX microprints, however, remain ordered and reproducible (fig. S4) with orientational errors within one degree and pattern dilations consistent to within of order one part in a hundred (fig. S5). Large surface area changes also accompany steep embossed reliefs (Fig. 1C.), which remain patternable by REFLEX printing but would similarly challenge other transfer techniques. With unlimited stretching, the reflow process can also pattern undercut structures with conventionally inaccessible overhangs (Fig. 1D) as well as adapt planar micropatterns to awkwardly shaped, macroscale objects. For example, Fig. 1E (and movie S1) demonstrate REFLEX microprinting not onto the proverbial pinhead but instead directly over the sharper tip. Similarly, fig. S6 shows transfer around a hypodermic needle point including within the lumen.

Conforming to non-planar surfaces does not always require stretching or reflow. A thin sheet can, for example, cover a cylinder or other developable surface of zero Gaussian curvature by bending alone; for suitable surface tension, γ, and bending modulus, B, the sheet may even spontaneously wrap the surface via capillary wetting, at least for radii of curvature exceeding the elasto-capillary lengthscale, $\sqrt{B/\gamma}$ (*15, 16*). Since B scales with thickness cubed, thinner sheets can wrap more tightly, but for the sheet wrapping to remain energetically favorable below microscale radii of curvature would require transfer carriers too thin to be mechanically practical (supplementary text). Even without microscale structure, however, many non-planar surfaces have non-zero Gaussian curvature. As exemplified by the mapmaker's dilemma projecting the spherical earth onto a flat page, for many mappings local area changes are therefore mathematically unavoidable. Truly conformal transfer then requires that any solid carrier not only bend, but also stretch. Unlike bending stiffnesses, however, stretching stiffnesses fall only linearly with reducing thicknesses (*15)*, thwarting conformal transfers onto intrinsically curved surfaces. By contrast, reflowable materials eliminate resistance to both bending and stretching, accommodating sharp, tightly curved features as well as transfer between widely differing Gaussian curvatures.

Such flexibility also allows REFLEX printing to maintain long-range order while deforming locally to cover non-planar features, as seen in the orderly array and diffracted colors of Fig. 1B. This preserved order suggests metamaterial or optical engineering of non-traditional surfaces (for

example, Fig. 1B), or materials, as in fig. S7, fig. S8, movie S2, and fig. S9, which show bendable, stretchable, and stimuli-responsive diffraction gratings created by transferring microarrays onto plastics, soft elastomers, and smart hydrogels, respectively.

For sufficiently small transfer structures, mapping transformations due to varying curvatures can be accommodated by dilating the spacings between structures rather than those structures themselves. But larger structures are also transferable (Fig. 2). While such structures might not themselves be stretchable (*17*), if thin, reflow can still guide their bending. The resultant 3-dimensional microprinting of continuously connected materials over edges (Fig. 2B) and around structures (Fig. 2C and movie S3) suggests possibilities for 3-d microfabrication or for 3-d integration in semiconductor manufacture. Locally transforming the carrier between solid and liquid via localized or directional heating (*12*) adds further control, enabling conforming or suspended constructions (Fig. 2D).

Because reflowing sugar gently envelops objects, naturally conforming without needing externally applied forces, REFLEX printing is also well suited for standalone microstructures, including those too fragile or tightly curved for other transfer methods. With reflow, microprinting over a self-standing strand of hair becomes comparatively undemanding for both small and relatively larger microstructures (Figs. 3A and 3B, respectively) but serves to demonstrate both micropatterning and microtexturing (Fig. 3C, (*12*)), as might be used to locally modify surface hydrophobicities. Or, scaling down in size, Fig. 3D and fig. S10 show printing onto more tightly curved fibers including a milkweed seed floss fiber and cellulose fibers within a sheet of paper, respectively. The high curvature, yet gentle, physicochemical attributes of the reflow process similarly support damage-free conformal printing over many other more complex biological surfaces. Examples include conformal transfer onto the corrugated surface of a poppy seed, into the subcellular-sized stomatal openings of a leaf, across increasingly tortuous, spiky surfaces of microscopic pollen grains and, for scale, over a red blood cell (Fig. 3, E, F, G, and H).

Higher curvatures imply higher surface area to volume ratios. High-curvature patterning should thus afford efficient, tailored microstructure control through printable surface functionalizations. Patterning microfibers, for example, at previously inaccessible sizescales and curvatures, adds functionality while maintaining structural flexibility and surface accessibility. As a simple illustration, gold-coated iron microdiscs transferred onto a milkweed floss fiber enable magnetic manipulation (Fig. 3D and movie S4)

At still smaller sizes, printing onto microparticles (Fig. 4) may influence biological responses to such particles (*18*) as well as advance sub-cellular sized biomedical probes, drug delivery vehicles, and microrobots (*19*). Microrobot miniaturization increases in-vivo access but fabrication and functional integration at necessary sizes and scales has remained challenging (*20*). Direct-write lithographies promise highly functional micromachines (*21*) but are hard to parallelize. Meanwhile, more scalable approaches, such as surface functionalizing microbeads, are constrained by existing high-curvature surface patterning abilities. By harnessing planar lithographies, REFLEX printing extends options beyond conventional homogeneous, Janus, or colloidal shadow or cluster-based designs (*22, 23*). As examples, Fig. 4, A, B, C, and D, show high-curvature transfer of a range of functional materials, shapes, and three-dimensional structures including: (i) gold disks, nickel rings, and platinum ellipses integrated on the same microspheres for possible localized biochemical functionalization or plasmonic heating, magnetic orientation, and catalytic self-propulsion (*24*), respectively, (ii) thick gold-coated iron cylindrical pucks for magnetic

manipulation or MRI-based tracking (*25, 26*), and (iii), as illustrations of higher aspect ratio transfers, cones and hollow cylinders incompatible with other transfer schemes due to fragility and / or the three-dimensional re-orientations needed for conformal mapping. In closely conforming to surfaces, the reflow process also increases contact areas between transferred patterns and receiving substrates, promoting clean, physical adhesion of REFLEX prints without needing externally applied placement pressure. For example, as shown in Fig. 4, E and F, of microspheres removed from their patterning substrate, centrifuged, washed and redispersed, at small sizescales prints can adhere directly through van der Waals forces without substrate modification. Moreover, for in-vivo usage biocompatible sugar-based manufacture adds no toxic solvents or transfer material residues.

The above transfers were randomly positioned but, as shaped hard candies attest, sugar can be molded, enabling surface embossed transfer media that double as their own guiding templates for massively parallel, automatic alignment of receiving substrates. As shown in Fig. 4G and fig. S11, sugar is here cast over transfer motifs patterned atop sacrificial photoresist posts. Resist dissolution then leaves those motifs within recessed wells in the carrier into which microbeads can self-assemble via capillary forces (*12, 27*). Reflowing, and subsequently dissolving, the carrier then conformally prints accurately registered transfers around potentially millions of separate substrates simultaneously (Fig. 4H). Removable stencils can also be similarly self-aligned for inverted etchings, functionalizations, or material depositions (Fig. 4, I and J), adding further possibilities for parallel printing of more arbitrarily designed colloidal “patchy” particles (28, 29).

The same sugar formulation has been used throughout, but it is neither unique nor necessarily optimal. Even regular store-bought candy suffices (fig. S12), raising the prospect of multiple alternative material formulations offering modified chemical and thermophysical properties, and further increasing accessibility of an already facile, inexpensive process. Such simplicity does, however, belie certain complexities of the reflow printing process. Firstly, while heating generally suffices for spontaneously conformal transfer, depending on surface energies, heated thin coatings can sometimes dewet rather than spread over a surface. If needed, wetting can be encouraged by pretreating the surface, applying gentle pressure, or using transfer layers a few millimeters thick to exceed any critical dewetting capillary lengthscales (*15*). Secondly, reflow over complex surfaces may trap air pockets, sealing off areas from pattern transfer. If necessary, directional heating (*12*) can help guide the reflow. Alternatively, provided material vapor pressures are low enough to limit gas bubble formation within the transfer material (fig. S13), heating in a vacuum oven not only evacuates the air but, if any sealed off areas remain, pressure differences on return to atmosphere help push the softened transfer material into these voids. Thirdly, at least for hygroscopic sugar-based materials, water absorbed from background humidity acts as a plasticizer, reducing T_g’s, even below room temperature. While this enables ambient heat-free reflow, absorbed water can also increase material vapor pressures and distort embedded transfer patterns. Conversely, subsequent shrinkage due to any evaporation from wet sugar layers can also distort transfers. Transfers not promptly redeposited onto receiving substrates may thus benefit from desiccator storage, which maintains dry sugar layers in a stable glassy state, preserving sub-micron pattern accuracy for months (fig. S14). Finally, despite broad compatibility across diverse substrate geometries and materials, work remains to ensure fully deterministic patterning over arbitrarily complex surfaces. While this work has focused on overcoming challenging surface topographies, reflow paths and, hence, mapping transformations, may depend also on locally varying surface chemistries. Here, targeted surface pretreatments or heating profiles may offer further control. Additionally, not unlike with conventional photolithographic proximity

corrections (*30*), initial pattern design modifications may compensate for anticipated mapping transformations.

References and Notes

1) A. Carlson, A. M. Bowen, Y. Huang, R. G. Nuzzo, J. A. Rogers, Transfer printing techniques for materials assembly and micro/nanodevice fabrication. *Adv. Mat.* **24**, 5284-5318 (2012).
2) C. Linghu, S. Zhang, C. Wang, J. Song, Transfer printing techniques for flexible and stretchable inorganic electronics. *npj Flex. Electron.* **2,** 26 (2018).
3) W.-H. Yeo, Y.-S. Kim, J. Lee, A. Ameen, L. Shi, M. Li, S. Wang, R. Ma, S. H. Jin, Z. Kang, Y. Huang, J. A. Rogers. Multifunctional epidermal electronics printed directly onto the skin. *Adv. Mat.* **25**, 2773-2778 (2013).
4) J. Park, Y. Lee, H. Lee, H. Ko, Transfer printing of electronic functions on arbitrary complex surfaces. *ACS Nano* **14**, 12–20 (2020).
5) M. A. Meitl, Z. T. Zhu, V. Kumar, K. J. Lee, X. Feng, Y. Y. Huang, I. Adesida, R. G. Nuzzo, J. A. Rogers, Transfer printing by kinetic control of adhesion to an elastomeric stamp. *Nat. Mater.* **5**, 33-38, (2006).
6) Z. Yan, T. Pan, M. Xue, C. Chen, Y. Cui, G. Yao, L. Huang, F. Liao, W. Jing, H. Zhang, M. Gao, D. Guo, Y. Xia, Y. Lin, Thermal release transfer printing for stretchable conformal bioelectronics. *Adv. Sci.* **4** 1700251 (2017).
7) G. F. Schneider, V. E. Calado, H. Zandbergen, L. M. K. Vandersypen, C. Dekker, Wedging transfer of nanostructures. *Nano Lett.* **10**, 1912-1916 (2010).
8) M. Aghajamali, I. T. Cheong, J. G. C. Veinot, Water-assisted transfer patterning of nanomaterials. *Langmuir* **34**, 9418-9423 (2018).
9) V. Linder, B. D. Gates, D. Ryan, B. A. Parviz, G. M. Whitesides, Water-soluble sacrificial layers for surface micromachining. *Small* **1**, 730 –736 (2005).
10) J.-A. Seo, S. J. Kim, H.-J. Kwon, Y. S. Yang, H. K. Kim, Y.-H. Hwang, The glass transition temperatures of sugar mixtures. *Carbohydr. Res.* **341**, 2516–2520 (2006).
11) B. Jiang, Y. Liu, B. Bhandari, W. Zhou, Impact of caramelization on the glass transition temperature of several caramelized sugars. Part I: Chemical analyses. *J. Agric. Food Chem*. **56**, 5138–5147 (2008).
12) Materials and methods are available as supplementary materials at the Science website.
13) D. Vella, L. Mahadevan, The "Cheerios effect". *Am. J. Phys.* **73**, 817-825 (2005).
14) A. Barbot, H. Tan, M. Power, F. Seichepine, G. Yang, Floating magnetic microrobots for fiber functionalization. *Sci. Robot.* **4**, eaax8336 (2019).
15) J. Bico, E. Reyssat, B. Roman, Elastocapillarity: When surface tension deforms elastic solids. *Annu. Rev. Fluid Mech.* **50**, 629–59 (2018).
16) D.-H. Kim, J. Viventi, J. J. Amsden, J. Xiao, L. Vigeland, Y.-S. Kim, J. A. Blanco, B. Panilaitis, E. S. Frechette, D. Contreras, D. L. Kaplan, F. G. Omenetto, Y. Huang, K.-C. Hwang, M. R. Zakin, B. Litt, J. A. Rogers. Dissolvable films of silk fibroin for ultrathin conformal bio-integrated electronics. *Nat. Mater.* **9**, 511-517 (2010).
17) J. A. Rogers, T. Someya, Y. Huang, Materials and mechanics for stretchable electronics. *Science* **327** 1603-1607 (2010).
18) S. Mitragotri, J Lahann, Physical approaches to biomaterial design. *Nat. Mater*. **8**, 15-23 (2009).
19) B. J. Nelson, I. K. Kaliakatsos, J. J. Abbott, Microrobots for minimally invasive medicine. *Annu. Rev. Biomed. Eng.* **12**, 55-85 (2010).
20) S. Palagi, P. Fischer, Bioinspired microrobots *Nat. Rev. Mater.* **3**, 113-124 (2018).

21) C. C. J. Alcântara, F. C. Landers, S. Kim, C. De Marco, D. Ahmed, B. J. Nelson, S. Pané, Mechanically interlocked 3D multi-material micromachines. *Nat. Commun.* **11,** 5957 (2020).
22) S.-M. Yang, S. G. Jang, D.-G. Choi, S. Kim, H. K. Yu, Nanomachining by colloidal lithography. *Small* **2**, 458-475 (2006).
23) Y. Wang, Y. Wang, D. R. Breed, V. N. Manoharan, L. Feng, A. D. Hollingsworth, M. Weck, D. J. Pine, Colloids with valence and specific directional bonding, *Nature* **491**, 51-55 (2012).
24) S. Sanchez, L. Soler, J. Katuri, Chemically powered micro- and nanomotors, *Angew. Chem. Int. Ed*. **54,** 1414-1444 (2015).
25) S. Martel, J.-B. Mathieu, O. Felfoul, A. Chanu, É. Aboussouan, S. Tamaz, P. Pouponneau, L. H. Yahia, G. Beaudoin, G. Soulez, M. Mankiewicz, Automatic navigation of an untethered device in the artery of a living animal using a conventional clinical magnetic resonance imaging system. *Appl. Phys. Lett.* **90**, 114105 (2007).
26) G. Zabow, S. J. Dodd, E. Shapiro, J. Moreland, A. P. Koretsky, Microfabricated high-moment micrometer-sized MRI contrast agents. *Magn. Reson. Med.* 65, 645-655 (2011).
27) Y. Yin, Y. Lu, B. Gates, Y. Xia, Template-Assisted Self-Assembly: A practical route to complex aggregates of monodispersed colloids with well-defined sizes, shapes, and structures. *J. Am. Chem. Soc.* **123**, 8718-8729 (2001).
28) M. He, J. P. Gales, E. Ducrot, Z. Gong, G.-R. Yi, S. Sacanna, D. J. Pine, Colloidal diamond, *Nature* **585**, 524-529 (2020).
29) Z. Zhang, S. C. Glotzer, Self-assembly of patchy particles. *Nano Lett*. **4**, 1407-1413 (2004).
30) A. Poonawala, P. Milanfar, Mask design for optical microlithography – An inverse imaging problem, *IEEE Trans. Image Process.* **16**, 774-788 (2007).

Acknowledgments: The author acknowledges useful discussions with Drs J. A. Liddle and S. Oberdick and thanks the anonymous reviewers for their comments and suggestions. **Funding:** This work was supported by National Institute of Standards and Technology (NIST) internal research funding. **Competing interests:** NIST has filed a provisional patent application on the reflow transfer print process. **Data and materials availability:** All data are available in the main text or the supplementary materials. This is a contribution of the National Institute of Standards and Technology, not subject to U.S. copyright.

Supplementary Materials

Materials and Methods

Supplementary Text

Figs. S1 to S14

Movies S1 to S4

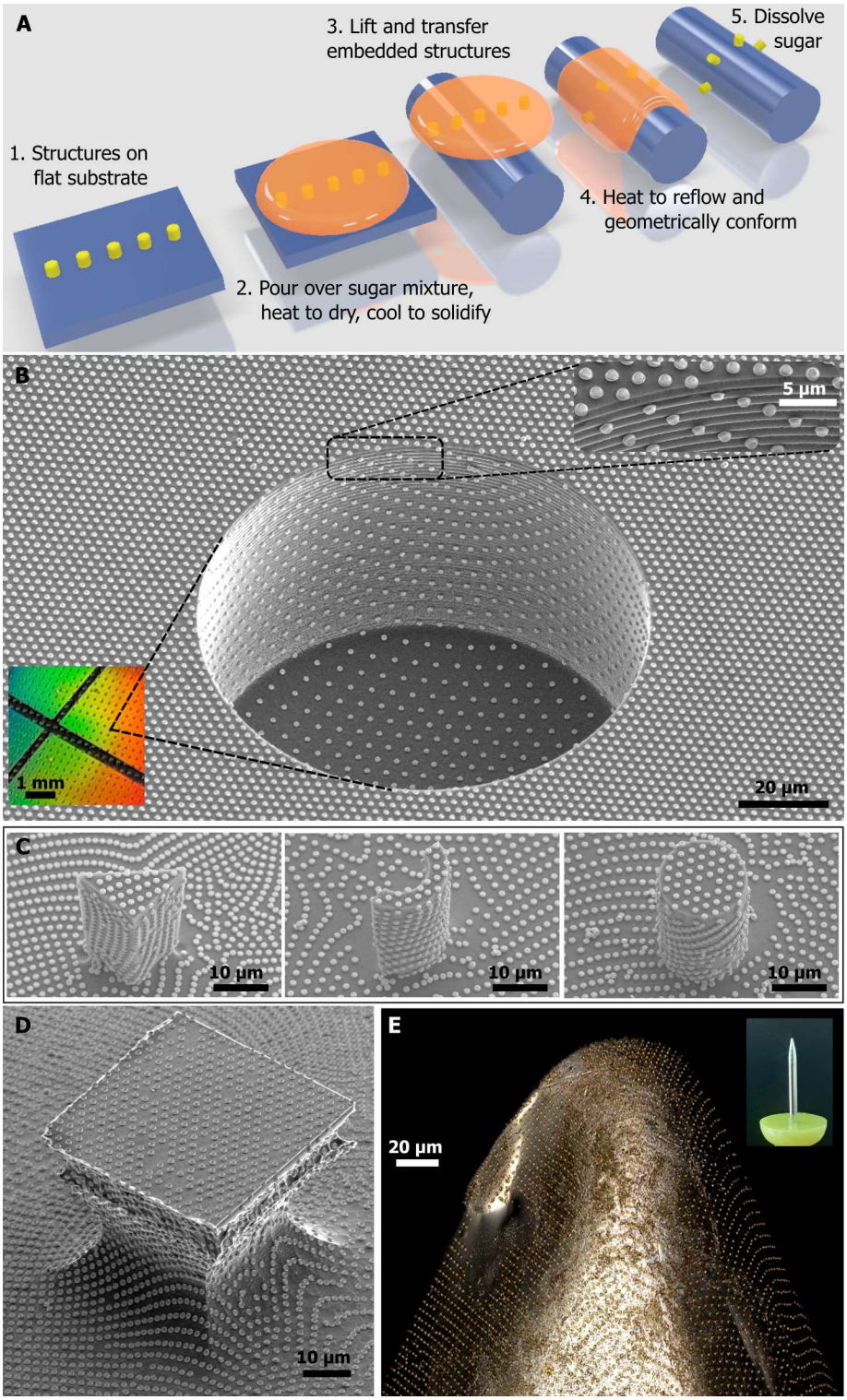

Fig. 1. Process schematic and example high-curvature conformal printing with reflowable materials. (**A**) Process steps, described in text, for structure transfer via reflowable materials that "melt" around the receiving substrate. (**B**) Scanning electron micrograph (SEM) of array of 1-µm disks transferred onto a surface with 100-µm diameter, 50-µm deep holes. Lower inset shows optical image of diffracted colors from transferred disk arrays; holes appear as dark spots. Upper inset shows magnification of pattern conformation over hole edge. (**C**) SEM's of disks transferred

onto sharp, vertical, high-aspect-ratio embossed features. (**D**) SEM showing transfer coverage of microstructure with multiple undercut regions. (**E**) Laser confocal optical micrograph of 1-μm disks transferred over the tip of a pin shown in the inset.

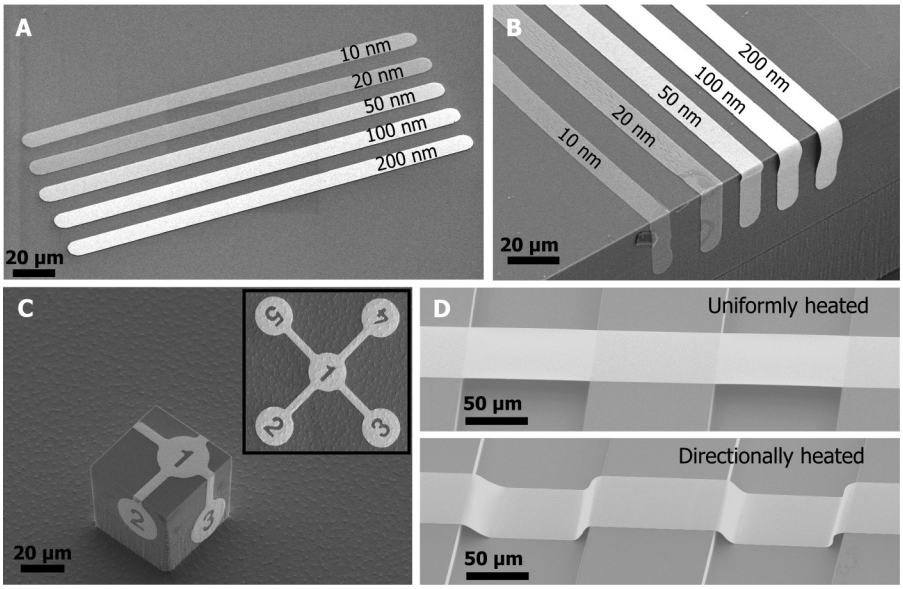

Fig. 2. Conformal transfer of extended structures. (**A**) SEM showing transfer of long, thin metal strips. Thicknesses as shown. (**B**) SEM of transferred structures of varying thicknesses (shown) wrapped around a sharp edge. (**C**) SEM of continuously connected printing around sides of a cube using 40-nm thick transfer structure simultaneously bent around multiple axes. Inset shows reference structure transferred onto a flat substrate. (**D**) SEM's of 100-nm thick metal strips printed across trenches, showing suspended (top) or conforming (bottom) placement, determined by controlling the reflow direction.

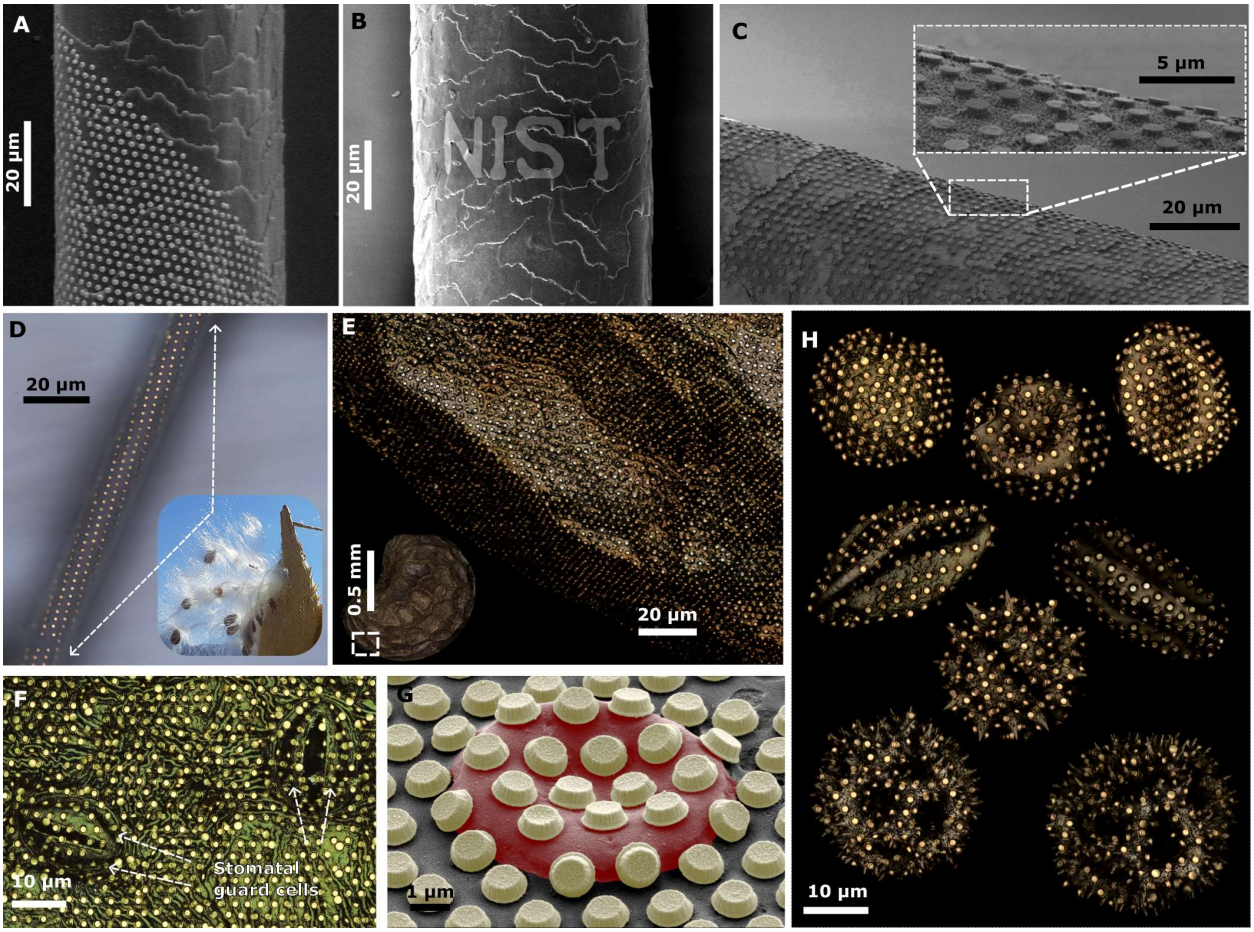

Fig. 3. Transfer patterning stand-alone microstructures. (**A**) and(**B**) show SEM's of 0.5-µm thick, 1-µm diameter Au disks and of 30-nm thick Au lettering, respectively, transferred onto individual strands of hair. (**C**) SEM showing surface microtexturing of a strand of hair, after ultrasonicating off transferred disks used as temporary oxygen plasma etch masks. Inset magnifies view of resulting texture. (**D**) Optical micrograph of 1-µm disks transferred onto a milkweed seed floss fiber. Inset shows milkweed seed pod, with floss fibers attached to seeds. (**E**) Laser confocal micrographs of a micropatterned poppy seed, including magnified view of lower boxed region detailing transfer printed disk array. (**F**) Laser confocal micrograph of the underside of a leaf, showing conformal pattern transfer including into the stomatal pores. (**G**) False-colored SEM showing the same Au disks used in (A, C, D, E, F, H) printed over a red blood cell for scale. (**H**) Collage of laser confocal micrographs of disk arrays conformally transferred onto various microscopic pollen grains of increasing surface complexity.

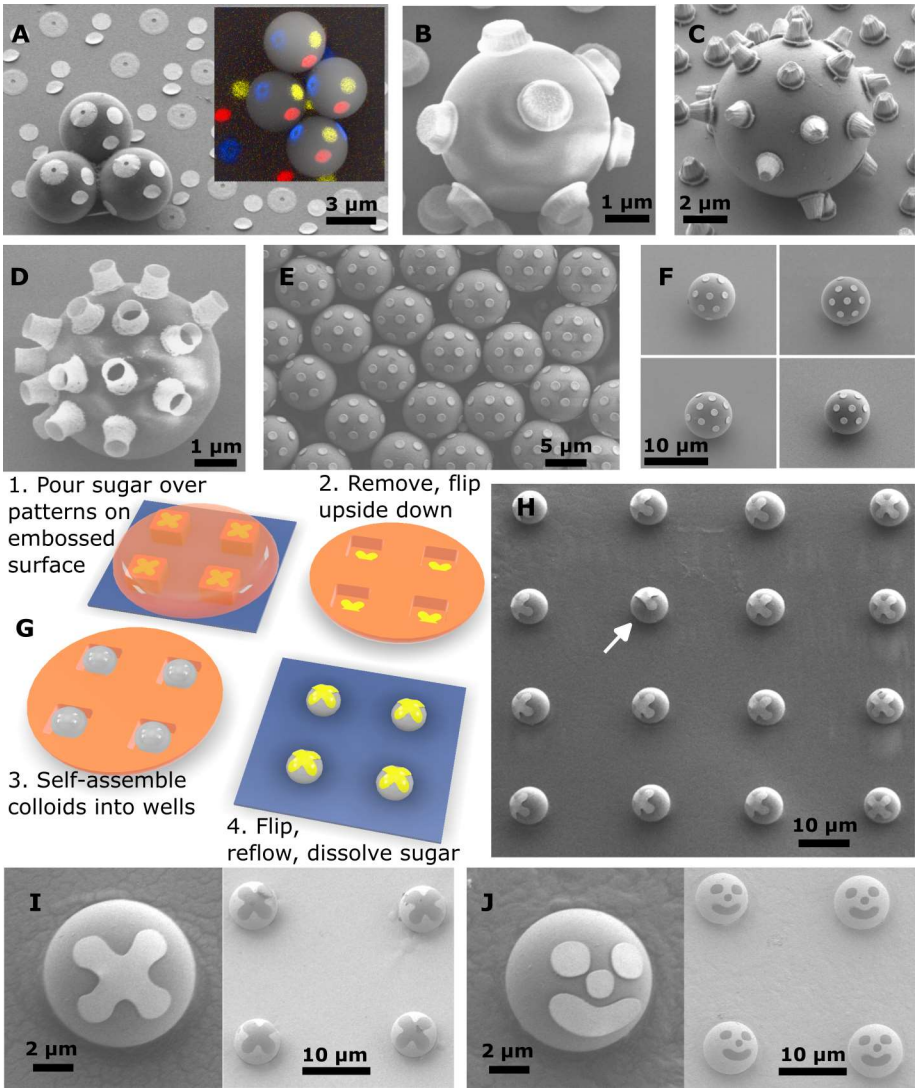

Fig. 4. Micropatterning colloids. (**A**) SEM of 4.5-µm polystyrene microspheres simultaneously transfer printed with multiple materials: Au disks, Pt ellipses, and Ni rings. Inset overlays color-coded energy dispersive X-ray spectroscopic scanned image on similar SEM to distinguish elements, revealing microsphere "faces" with red (platinum) "mouths", yellow (gold) "noses" and blue (nickel) "eyes". (**B**) SEM of 1-µm diameter, 0.5-µm thick, gold-coated magnetic iron disks transfer printed onto polystyrene microsphere. (**C**) SEM of gold cones (1-µm base diameter, 1-µm tall) transferred onto a 7.5-µm glass microsphere. (**D**) SEM of hollow 500nm-diameter cylinders transferred onto polystyrene microsphere. (**E**) SEM of as-patterned, and (**F**), subsequently redispersed microspheres showing robust print attachment. (**G**) Schematic for parallel, self-aligned transfer printing. (**H**) SEM of cross patterns transfer printed in parallel onto array of glass microspheres. (arrow shows a folded-over defective transfer) (**I**) SEM's of patterned microsphere and its inverses created using original print as temporary mask for subsequent metal deposition. (**J**) as in (I), except with multi-piece transfer design.

Supplementary Materials for

Reflow transfer for conformal 3-dimensional microprinting

Gary Zabow

Correspondence to: gary.zabow@nist.gov

This PDF file includes:

Materials and Methods
Supplementary Text
Figs. S1 to S14

Other Supplementary Materials for this manuscript include the following:

Movies S1 to S4

Materials and Methods

The reflow transfer printing process

i) Sugar mixture

Sugar mixtures were made from 2 parts sugar mixed with 1 part corn syrup and 1 part deionized (D.I.) water and then heated to caramelization, around 170 °C -180 °C. No specialty chemicals were used; sugar and corn syrup were purchased from the bakery aisle of a regular grocery store. Different degrees of caramelization, as shown with the different resulting solution colors in fig. S1, D, E, and F, will result depending on the exact temperature and time that the sugar mixture is kept at that temperature. Although caramelization degree does affect the resulting glass transition temperature, this variable has not been optimized yet since it was found that all three levels of caramelization in fig. S1 worked suitably for transfer printing.

The solution solidifies on cooling to room temperature after which it is dissolved 1:1 with D.I. water. This final sugar-water solution can then be stored for months to be used as needed.

ii) Coating the transfer patterns with sugar

The diluted solution is poured over transfer structures, generally pre-fabricated on an acetone-soluble sacrificial layer, itself spun onto a silicon support wafer. To avoid runoff, the wafer is taped around its edge as shown in fig. S1A. Generally, 5 ml to 10 ml of the above sugar-water solution provided a suitable thickness coverage over a 76 mm (3-inch) wafer. This solution is slowly heated to remove water until the solution viscosity increases enough that it does not run off the wafer when the tape is removed. (Fast heating was avoided because it led to bubbles forming in the solution). The solution is then further heated to more fully dry out the sugar layer. Heating times and temperatures depend on the thickness of the sugar layer prepared. As a starting guide, leaving the wafer in an oven overnight near 100 °C was generally sufficient for 5 ml to 10 ml's worth of solution. Thicker layers, or lower temperatures, may require more time; conversely, if the substrate and transfer features permit, higher temperatures and shorter times can be used. After drying, the wafer is allowed to cool slowly (to avoid cracking the sugar layer) leaving a dried, hardened sugar layer as shown in fig. S1B.

The amount of water remaining in the sugar layer has significant effects on the subsequent behavior of that sugar layer. Too much water will leave a layer that is too sticky to remove from the wafer or one that, while it can be removed from the original substrate, may immediately stick to the receiving substrate on contact, complicating accurate positioning on that receiving substrate; drier sugar layers are not sticky and can easily be maneuvered for accurate positioning on receiving substrates, but very low water contents can make for brittle layers that require more careful handling to avoid cracking. Water content also determines the glass transition temperature and vapor pressure of the final sugar layer (important if attempting vacuum-assisted transfer printing, described below).

iii) Releasing the sugar layer

If using a sacrificial layer, the sugar-coated wafer is submerged in acetone to dissolve that layer. The time required for this can vary substantially based on how much water was remaining in the sugar layer: the wetter the sugar layer, the longer this process takes, to the point that particularly sticky layers may never release. Also, since the acetone access to the sacrificial layer is diffusion limited, release time can vary quadratically with the size of the layer. However, for very dry layers, presumed residual stress in the sugar layer seems to help it peel itself off the substrate, helping to expose the sacrificial layer and leading to a far more rapid release process. For a 76mm (3-inch) wafer, release can therefore vary from under a minute (very dry sugar) to over a week (wetter sugar).

For very dry sugar layers, however, a sacrificial layer may not be needed at all. Dry sugar layers can often be popped off the substrate simply by carefully wedging a razor blade under an edge to start the process, which is again presumably helped by residual stress in the solidified sugar layer. Alternatively, if the sugar is poured over a flexible surface as opposed to a rigid silicon wafer, that substrate can often be peeled off without any sacrificial layer being required.

For reference, a released sugar layer is shown in fig. S1C.

Sacrificial layers used were either Megaposit SPR660 photoresist spincoated and partially hardbaked at 150 °C for 5 minutes, or 950 PMMA A4 e-beam resist spincoated and baked at 180 °C for 2 minutes, but any other acetone soluble materials or resists would likely work too.

iv) Transfer onto receiving substrate

Patterns are transferred onto receiving substrates by gently heating the sugar layer. Depending on the glass transition temperature, and on the time that the sugar is left in contact with the receiving substrate (i.e. the time given to reflow), temperatures as low as 35 °C to 40 °C may suffice, but higher temperatures can also be used to speed up the process and/or enable reflow around sharper features. After this, the sugar is dissolved away in water.

In cases where a sacrificial release layer was used and the wafer was soaked in acetone, a very thin, nanometers-level thickness, water-insoluble layer was sometimes found coating the surface of the released sugar layer. Its composition is unclear, but it presumably results from some residue from, or surface reaction with, the acetone. This layer can impede truly conformal transfer as well as leave an undesired residue on the receiving substrate. Fortunately, the layer is easily removed by exposing the released sugar layer to an oxygen plasma for a couple of minutes before proceeding to place, and reflow, the sugar over the receiving substrate. The plasma system used should either be actively cooled, or if necessary, the plasma ashing done in steps to ensure minimal heating of the sugar layer. Note that this plasma treatment is on the sugar layer only; the receiving substrate need not be exposed and thus it does not in any way contaminate or limit the allowable receiving substrate materials. Note also that the receiving substrate never comes into contact with the acetone solvent either; it sees only sugar and water. Additionally, when dry releasing the sugar layer without needing to dissolve a sacrificial layer, no such surface residue was found and thus no oxygen plasma was required.

v) Reflow transfer with directional heating

Generally, heating is applied uniformly across the sugar layer, using either a hotplate or oven. This leads to the sugar softening and reflowing simultaneously across the substrate. In some cases, however, having the sugar start to reflow in one location before another, may be desirable to control the reflow printing process. An example is shown in Fig. 2D. With uniform heating, as the sugar reflows, the transferred metal strip attached to the sugar layer first contacts the receiving substrate surface on the raised edges on either side of the trench, before the sugar reflows down into the trench. Since the metal strip is not itself stretchable, however, once it is pinned on either side of the trench it cannot lengthen itself to contact the bottom of the trench. This yields a suspended structure transfer. However, if the reflow process happens first on, say, the righthand side of the trench and then proceeds through the trench to the lefthand side, then the metal strip is initially pinned only on the top righthand edge of the trench and can, if thin and bendable, follow the reflowing sugar down into the trench and up out on the other side. If using a hotplate, such directional reflow can be achieved simply by placing a thermally insulating spacer (for reference, a piece of wooden toothpick was used to create the result shown in Fig. 2D) under one edge of the sugar layer when it is laid down on the receiving substrate. With heat only coming up from the hotplate beneath, the sugar reflow will occur first at the point where the sugar is making direct contact with substrate before proceeding across to the side of the spacer where the sugar is more distant from the heating source. Alternatively, directional reflow can be achieved by appropriately directing a heatgun at the sugar layer. Similarly, control over the local reflow process could likely also be achieved with a conveyer belt oven or more accurately by using a heating laser directed at the point(s) where reflow is required.

vi) Reflow transfer under vacuum

Certain challenging geometries may trap air pockets and prevent the sugar mixture locally from contacting areas on the receiving substrate. This can often be overcome either through directional heating or by heating in a vacuum oven. Here the relative moisture in the sugar layer is important since higher moisture content implies higher material vapor pressures. As with most materials, heating increases the sugar vapor pressure and, if it contains too much moisture, this may cause gas bubble formation within the sugar layer as it is being heated under vacuum but before it has heated enough to reflow sufficiently (see fig. S11). If at the interface between the sugar and receiving substrate, these bubbles can distort the pattern transfer. The drier the sugar layer, the lower its vapor pressure and the higher the temperature that can be reached before bubbling occurs. The only example in the manuscript that used vacuum transfer was the hole patterning in Fig. 1B (and figs S2 and S3); without vacuum it was consistently found more difficult to fully pattern the bottom of the holes.

vii) Reflow transfer surface microtexturing

Transferred patterns can be used as their own masks for subsequent processing. This is seen in the inverted patternings of Fig. 4, I and J, as well as in the surface texturing of Fig. 3C. Both require removing the transferred patterns from the substrate after the subsequent processing. This can be achieved by ultrasonicating the patterns off, or by using patterns made of a material that can be selectively etched / dissolved. As an organic material, for the strand of hair shown in Fig. 3C, texturing was achieved by O_2-ashing the hair, which was patterned with thick gold

disk masks, in an oxygen plasma before ultrasonicating it to remove the original pattern layers. Longer ashing times yield increased surface texture.

viii) Self-aligned, massively parallel transfer printing

The automatically aligned microsphere patternings seen in Fig. 4, H, I, and J were created using a modified version of template-assisted self-assembly (TASA). The TASA process, first developed in ref. 28, uses a moving liquid front to drag microspheres within that liquid over a surface. If that surface has appropriately sized wells, the microspheres can be pushed into those wells as they are dragged over the surface while other microspheres are carried away, leaving a regular spaced array of microspheres. Typically, this process uses water as the carrier fluid, but here acetone was used instead so as not to dissolve the wells in the sugar surface template. The efficiency of the process is known to depend on multiple parameters, such as the fluid layer's wetting contact angle, evaporation rates, and the speed at which the fluid front moves. However, for the proof-of-principle demonstrations shown in Fig. 4, H, I, and J, none of these parameters were optimized yet; rather, microbeads were simply mixed in with acetone and a few droplets of the solution placed on the sugar well template surface with a microscope cover slip immediately dropped on top. Evaporation of the acetone out the sides underneath the cover slip then led to the necessary moving fluid front. Accordingly, there remains much room to optimize this process.

Once all the acetone had evaporated the cover slip was removed, and the sugar template, with the microbeads in the wells, was heated to reflow and transfer the patterns at the bottom of the wells onto the microbeads, before being dissolved away in water.

Equipment used

- All laser confocal microscopy was performed on a Keyence VK-X1100 3D optical profilometer.
- Scanning electron microscopy images were acquired on either a FEI Sirion SEM or a Zeiss Sigma 300 SEM, depending on availability. Energy dispersive X-ray measurements were performed on the same Zeiss Sigma 300 using a Zeiss SmartEDX Detector.
- Sugar heating was performed on either standard laboratory hotplates or ovens (with a vacuum port connection for the vacuum assisted transfer)
- Holes and embossed test features on silicon wafers were all created through Bosch process deep reactive ion etching (DRIE) using an STS ASE DRIE.
- All lithographic patterning of test transfer structures was done using either an ASML 5500 Wafer Stepper (with pattern masks made in house using a Heidelberg DWL2000 Pattern Generator) or a Heidelberg MLA 150 maskless aligner.
- Test transfer structures metals were all deposited using one of two vacuum e-beam evaporators (one from Kurt Lesker, one from AJA International) depending on availability.
- Oxygen plasma ashing was done in either a water-cooled Technics PE-IIA plasma system or a Tergeo plasma cleaner (Pie Scientific).

Other materials

- The polydimethylsiloxane used in fig. S6 and movie S2 was Sylgard 184 (Ellsworth Adhesives) cured by heating in the standard 10:1 curing agent ratio.
- The pH sensitive hydrogel used in fig. S7 was made from a precursor solution containing a 1:1 ratio (w/w%) of poly(ethylene glycol)(n) dimethacrylate (with a poly(ethylene glycol) block molecular weight of approximately 200, Polysciences) and methacrylic acid (Sigma-Aldrich). To this was added 5% (w/w%) of 2,2-dimethoxy-2-phenylacetophenone (Sigma-Aldrich), used as a photo-initiator. UV cross-linking was performed under nitrogen.
- Polystyrene and glass microbeads seen in Fig. 4 were acquired from Polysciences and from Cospheric Microspheres, respectively.
- Pollen grains were harvested from random wildflowers growing alongside Colorado hiking trails, but any pollen would do.
- Candy used in fig. S10 was all Jolly Ranchers hard candies.

Note that the above equipment, candy, and chemical supplier names are included solely to specify experimental details; they do not indicate National Institute of Standards and Technology (NIST) endorsement of any particular company or product.

Supplementary Text

Capillary wetting curvature limit

The minimum radius of curvature, R, that can be wrapped by capillary wetting with a fluid of surface tension, γ, for a sheet of bending modulus B, scales with the elastocapillary length as

$$R \sim \sqrt{B/\gamma}$$

For a thin plate / sheet geometry:

$$B = Et^3/12(1-\nu^2)$$

where E is the Young's modulus, ν is the Poisson ratio, and t is the thickness of the sheet. Substituting into the elastocapillary length above, and solving for the sheet thickness required to allow wrapping about a certain radius of curvature, gives:

$$t(R) \approx \sqrt[3]{\frac{12R^2(1-\nu^2)\gamma}{E}}$$

Assuming a Poisson ratio near 1/2 and using the surface tension of water, $\gamma = 72$ mN m^{-1}, gives

$$t(R) \approx \sqrt[3]{\frac{R^2}{E}}$$

Thin films used as backing support or as transfer carriers generally include various polymeric materials, most commonly: poly (methyl methacrylate) (PMMA), polyvinyl alcohol (PVA), poly (L-lactic acid) (PLLA), polyimide (PI), polyethylene terephthalate (PET), and silk. All have Young's moduli in the range of 1 – 5 GPa. For a best-case scenario of 1 GPa, the sheet thickness required to wrap a cylinder of radius R, becomes:

$$t(R) \approx \frac{R^{2/3}}{1000} \text{ [m]}$$

That is, to wrap around a feature with 1-micrometer radius of curvature via capillary wetting, requires a sheet thickness of order 100 nm, mechanically challenging to support without damage or wrinkling for any appreciable size of sheet; tightly wrapping smaller radii of curvature, such as those associated with sharp feature edges for example, quickly becomes increasingly impractical.

(Note: another common transfer material, polydimethylsiloxane (PDMS), is more flexible than the above polymers with a Young's modulus of order 1 MPa; however, transfer printing with PDMS requires much thicker layers for mechanical stability of the PDMS, rendering it unsuitable for bending around high curvatures).

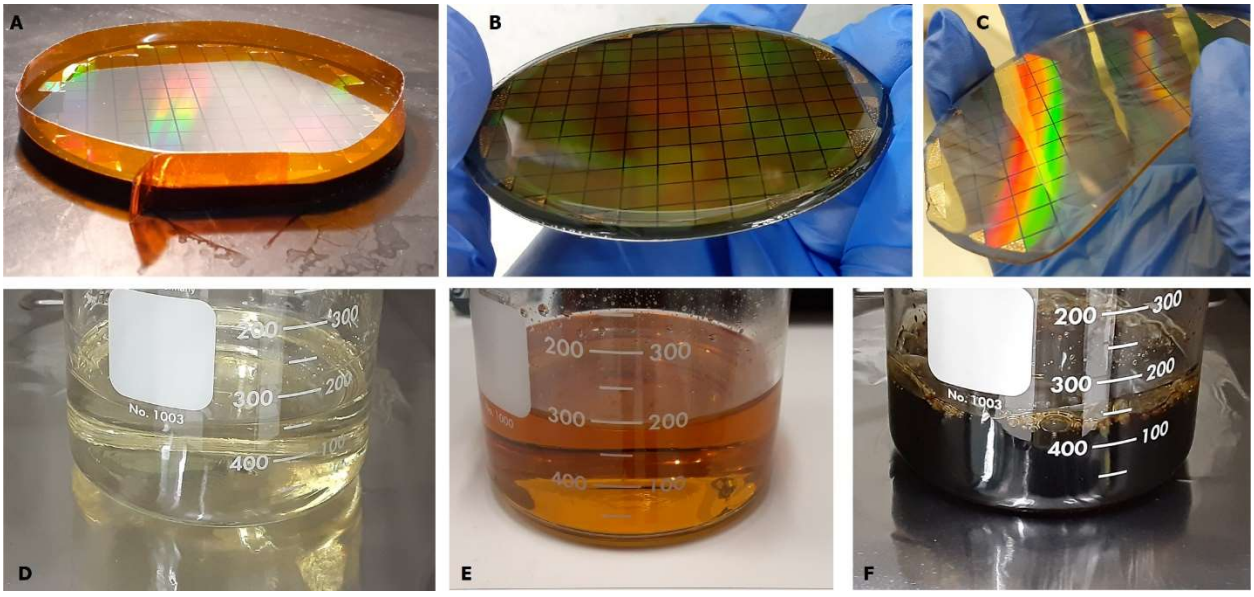

Fig. S1.

Steps in the transfer patterning process. (**A**) shows a 76 mm (3-inch) silicon wafer hierarchically patterned with arrays of 1-μm diameter disks that are to be transfer printed. Each square is 5.12 mm on a side and contains ~ 5 million disks arrayed in a 2d hexagonal lattice with center-to-center spacing of 2.5 μm. Colors are due to optical diffraction off the arrays. Tape is placed around the wafer to form walls making a container into which the sugar solution can be poured to temporarily retain it while water in the solution is evaporated by heating. This tape is removed partway through the evaporation process, once the solution is viscous enough to no longer flow over the edge of the wafer and the heating process then continues until the sugar solution has dried out more fully. (**B**) Image of the wafer with a dried, hardened coating of the sugar mixture. (**C**) Image of the disk arrays attached to the sugar layer after the sugar layer has been removed from the silicon wafer and is ready for transfer onto the chosen receiving substrate. The solid sugar layer is broken to show its cross section. (**D**), (**E**), and (**F**) show the liquid sugar mixture itself, being prepared with increasing degrees of caramelization from left to right, visible through the increasingly darker color of the mixtures.

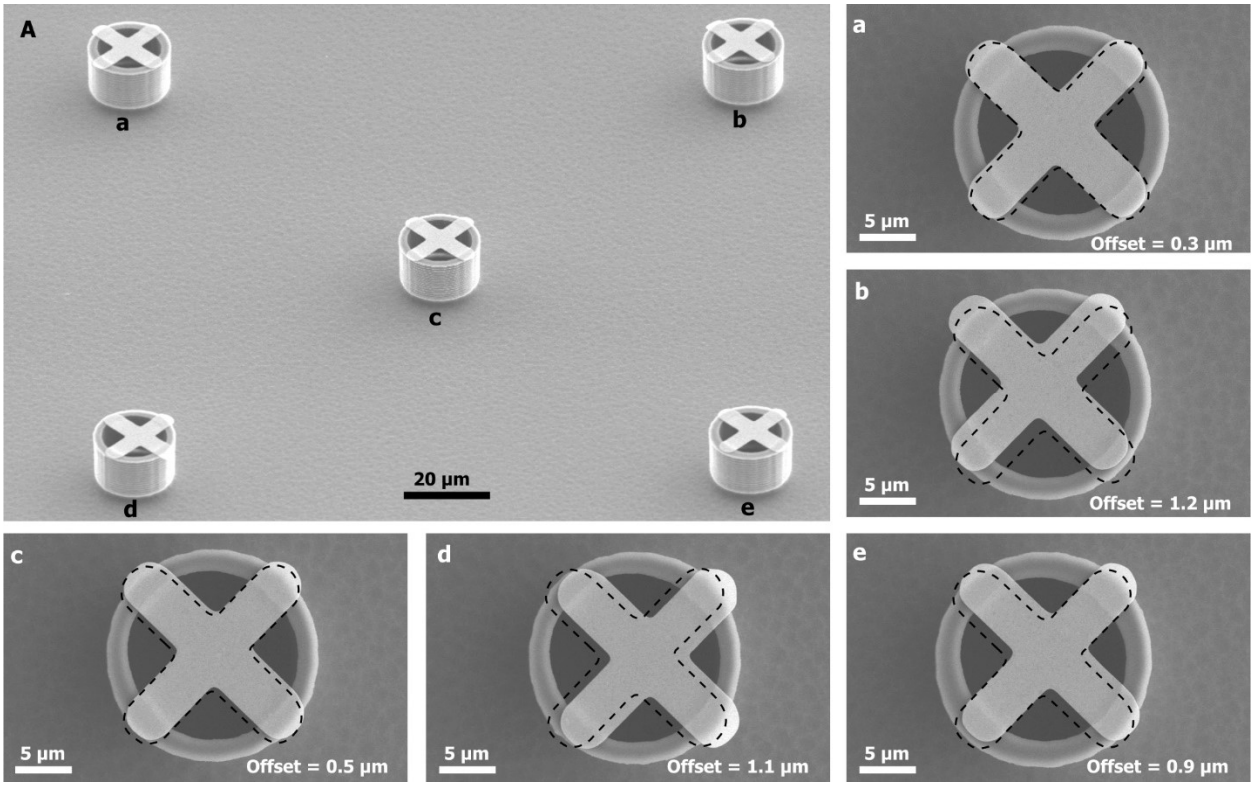

Fig. S2.

Transfer placement accuracy. (A) Angled scanning electron micrograph (SEM) showing 50-nm thick, 20-µm wide, gold crosses simultaneously REFLEX printed (and suspended) on top of hollow vertical posts. Surrounding panels show top-down SEMs of each cross on each post, as labeled in (A), with ideal centered cross positions denoted by dashed outlines. Offsets show experimental deviations from these targeted positions falling within ~ 1 µm.

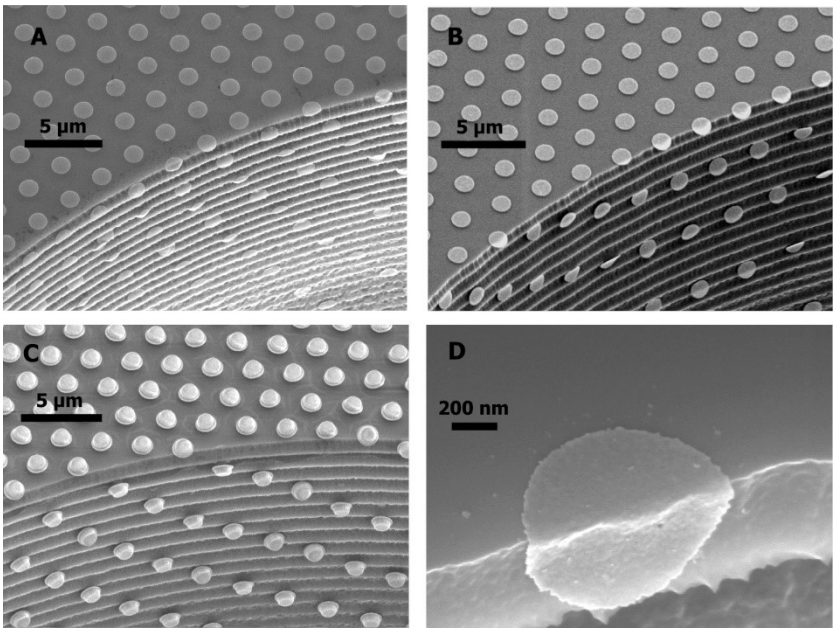

Fig. S3.

Transfer of flexible and rigid structures around sharp edges. (**A**), (**B**), and (**C**), angled scanning electron micrographs of arrays of 1-µm diameter disks of 10 nm, 35 nm, and 500 nm thicknesses, respectively, transfer printed over the edge of a hole etched into a silicon wafer (similar to that shown in Fig. 1B). The 10 nm disks completely wrap the surface including bending conformally over the hole edge as well as over the sharp ridges that extend down the hole side wall. The thicker 500 nm disks are themselves too rigid to bend, but the transfer process leads to them still closely follow the surface, including changing their orientation to match the ridges as needed. The 35 nm disks show behavior averaging that of the thin and thick disks: they partially bend, as well as reorient to match the top edge and ridges. (The repeating ridge lines in the vertical sidewalls are a consequence of the cyclic nature of the deep reactive ion etching (DRIE) Bosch process used to create the holes). (**D**) Higher magnification view of a 10-nm thick 1-µm diameter disk transfer printed over the top rim of a hole showing the sharp, nanoscale curvature of the edge.

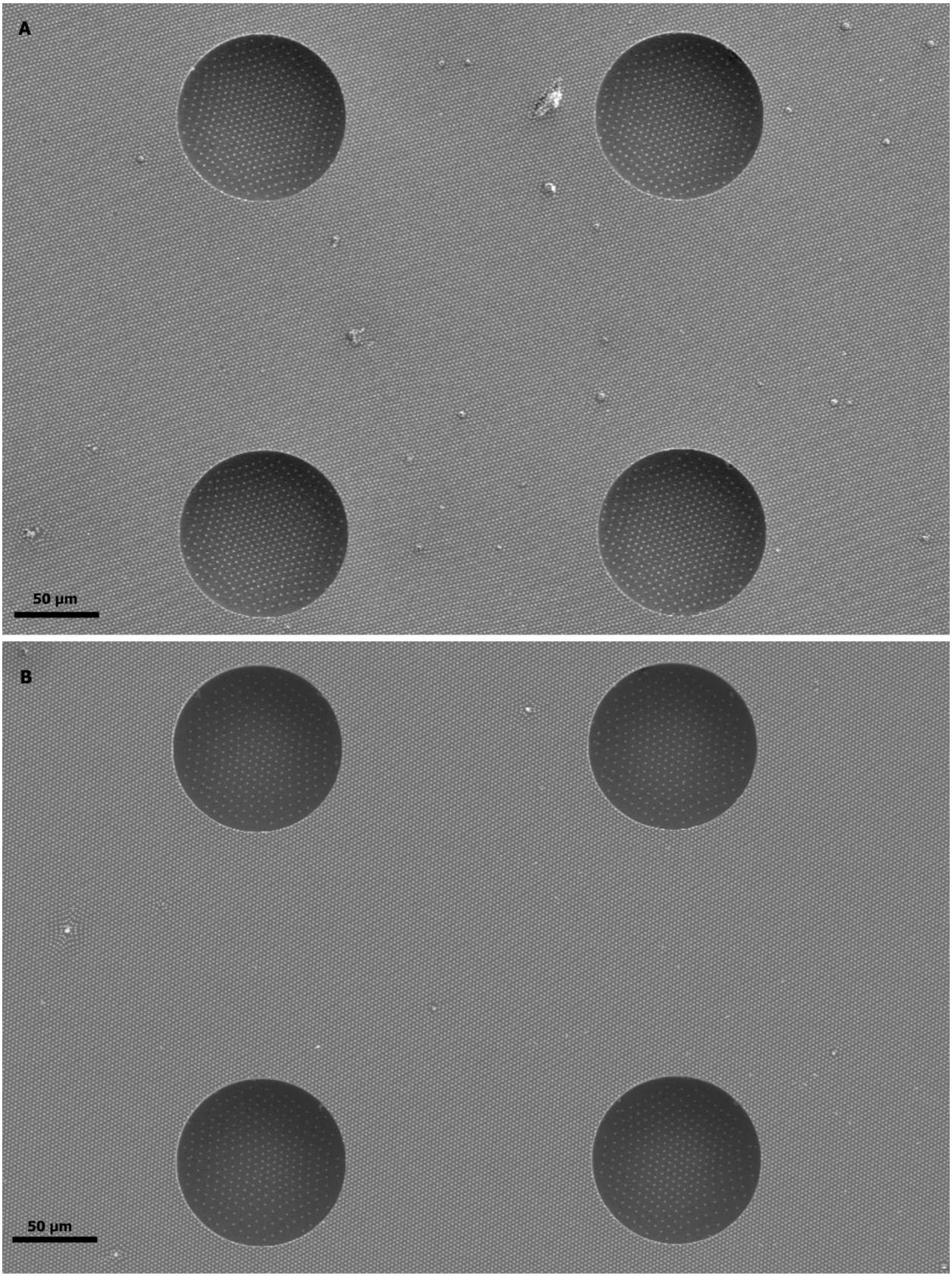
A
50 µm
B
50 µm

Fig. S4.

Transfer reproducibility and maintenance of array order. (**A**) and (**B**), top-down scanning electron micrographs of array of 1-μm disks (center-to-center array spacing, 2.5 μm) transfer printed onto silicon wafers with 100-μm diameter holes. The local increase in substrate surface area due to the additional sidewalls forming the holes leads to stretching of the array pattern spacings within the holes compared to the undisturbed spacings surrounding the holes. The holes are 50-μm deep in (A) and 75-μm deep in (B), leading to a tripling, and quadrupling of the local areas, respectively, and an accordingly greater stretching of the array spacings in (B) versus those in (A). Each image shows a set of 4 holes to demonstrate the preservation of array order and reproducibility of the printing coverage and stretched array patterns.

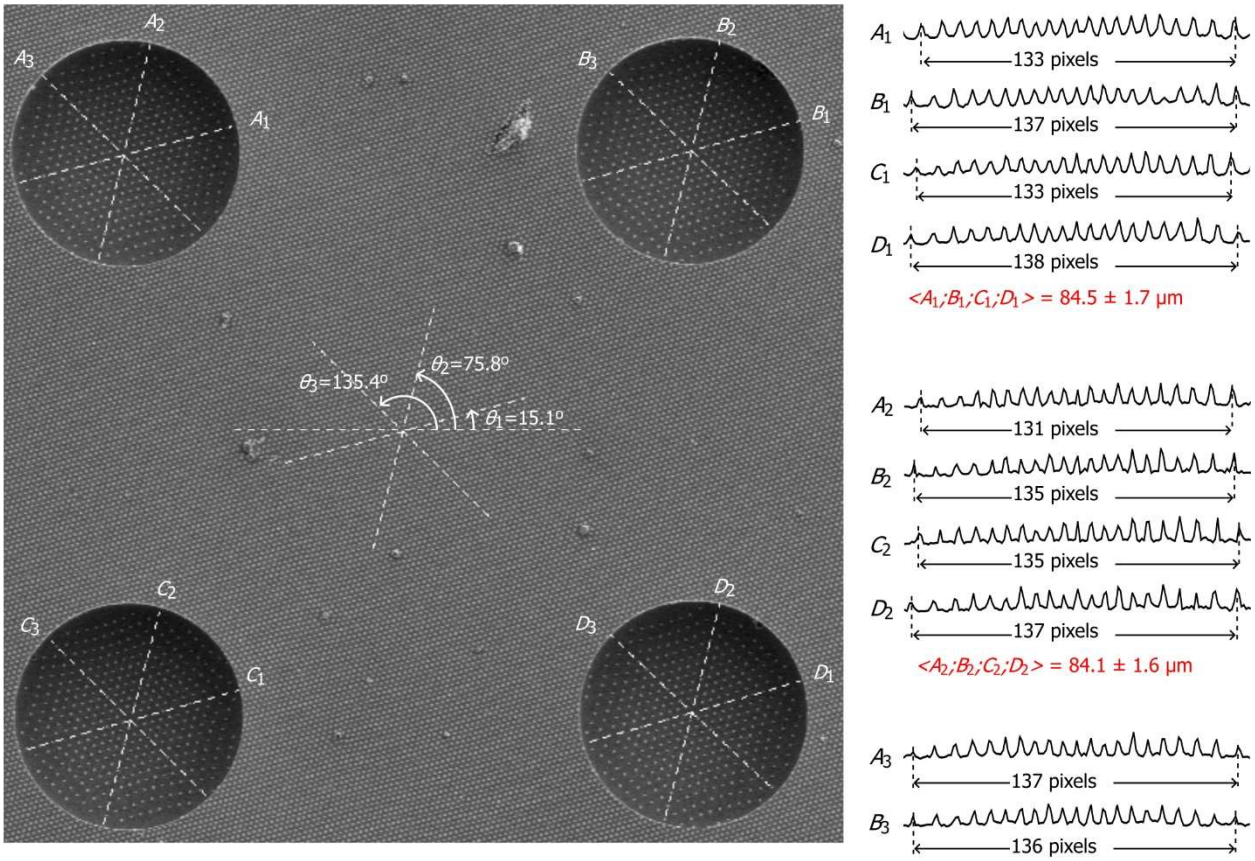

	θ	Δθ=/θ - θ1/
A1	14.7°	0.4°
B1	15.6°	0.5°
C1	15.5°	0.4°
D1	16.0°	0.9°

	θ	Δθ=/θ - θ2/
A2	76.5°	0.7°
B2	75.5°	0.3°
C2	75.2°	0.6°
D2	75.6°	0.2°

	θ	Δθ=/θ - θ3/
A3	135.5°	0.1°
B3	136.2°	0.8°
C3	135.1°	0.3°
D3	136.5°	1.1°

Fig. S5.

Quantitative transfer mapping repeatability. Main panel shows scanning electron micrograph, reproduced from fig. S4A, with overlaid dashed lines to indicate positions and angles of cross-sectional line cuts taken across the stretched transfer prints at the bottom of the holes. Also shown are the angles that the main axes of the original transfer printed, but unstretched, hexagonal array make with a horizontal reference. Measured orientation angles, Θ, of the array axes within each hole, and their deviation, $\Delta\Theta$ (red), from the unstretched array are shown below. The image linecuts through each hole, each extending out to the 10th transferred disk on either side of the centermost disk in each hole, are shown alongside. Distances spanned by each set of 21 disks are measured in pixel counts. Average distances together with standard deviations in those distances (red), scaled in terms of micrometers, quantify the reproducibility of the reflow stretching across the separate holes.

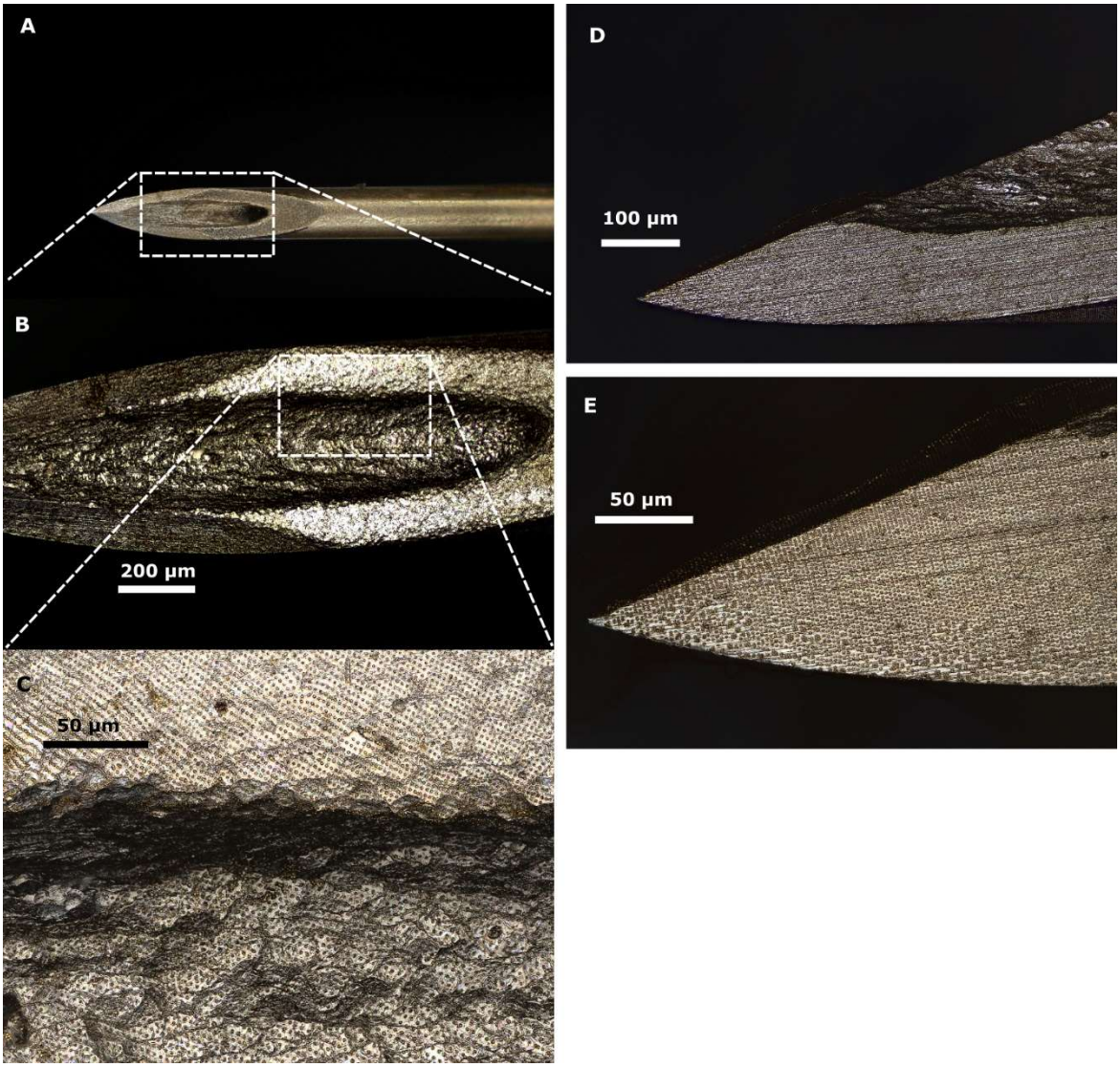

Fig. S6.

Transfer onto a hypodermic needle. (**A**), (**B**), and (**C**) are a series of top-down laser confocal micrographs of increasing magnification of an array of 1-um disks transferred printed onto the sharp end of a hypodermic needle, showing ordered pattern coverage extending within the concave, recessed lumen. (**D**) and (**E**) show different magnification side-view laser confocal micrographs of patterning at the tip of a hypodermic needle.

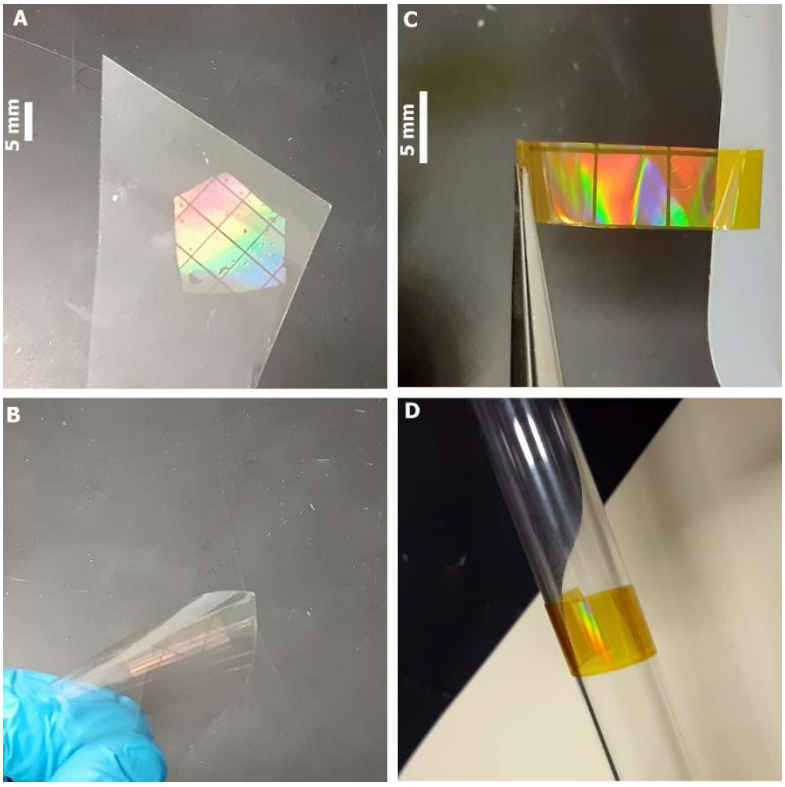

Fig. S7.

Transfer onto plastics. Hierarchical patterning of arrays of 1-μm gold disks transferred onto (**A**) a piece of plastic, shown bent in (**B**) to demonstrate material flexibility, and (**C**) a piece of plastic tape, similarly shown subsequently bent (and taped) around a tube in (**D**).

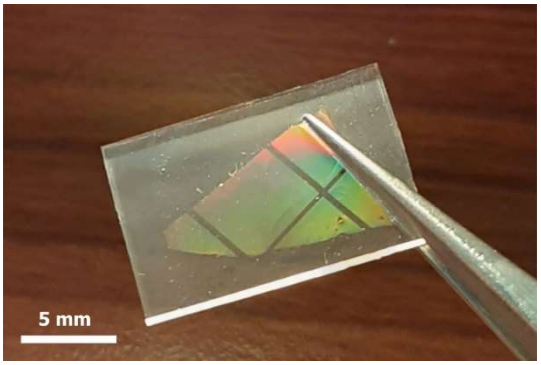

Fig. S8.

Diffraction grating transferred onto elastomer. Arrays of 1-μm gold disks (hexagon array center-to-center spacing, 2.5 μm), transferred onto a thin, flexible, polydimethylsiloxane (PDMS) substrate to be used as mechanically stretchable optical diffraction grating (see movie S2).

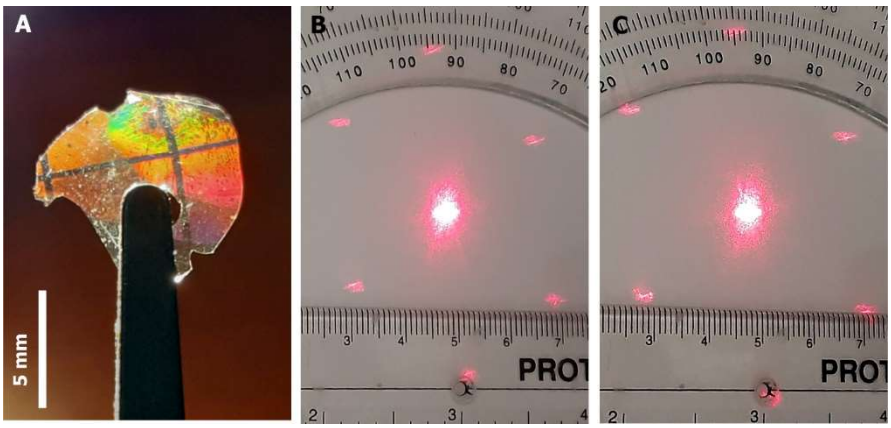

Fig. S9.

pH sensing by transfer printing onto stimuli-responsive hydrogel. (**A**) A thin sliver of an acid-sensitized, poly(ethylene glycol) dimethacrylate (PEGDMA) hydrogel, covered in transfer printed arrays of 1-μm diameter, 2.5-μm center-to-center spacing, disks. (**B**) and (**C**), optical diffraction from a laser pointer shone through the hydrogel when it is submerged in a pH 6 and a pH 5 buffer solution, respectively. The acid sensitive hydrogel shrinks as the pH drops, leading to a reduction in the spacing between the transfer printed disks and an according increase in the resulting diffraction angles and diffracted spot spacings, as can be seen by comparing the relative spacing of the diffracted spots visible in (B) and (C).

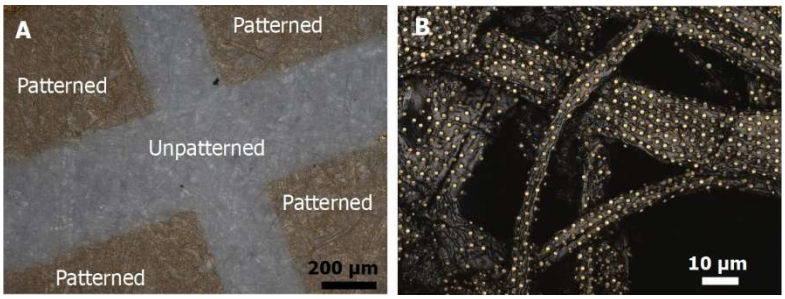

Fig. S10.

Transfer onto paper. (**A**) Optical microscope image of hierarchically patterned arrays of 1-µm gold disks transferred onto a sheet of paper. (**B**) Laser confocal micrograph of a magnified region of the paper showing transferred pattern conformation about the cellulose fibers within the sheet of paper.

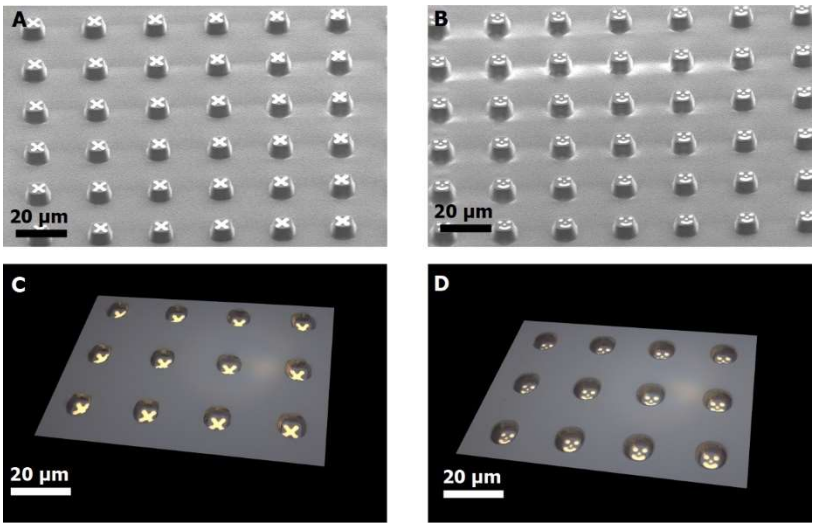

Fig. S11.

Transfer patterns prepared on embossed surface posts and within recessed sugar wells. (**A**) and (**B**), angled scanning electron micrographs showing thin-film metallic patterns, to be used for transfer printing, prepared atop embossed photoresist posts. (**C**) and (**D**), 3-dimensionally rendered laser confocal micrographs of sugar layers that have been cast over, and subsequently removed from, the substrates shown in (A) and (B), respectively. The metallic patterns to be transferred, which were on the tops of the embossed post, are now visible at the bottom of the wells that have been molded into the sugar surface and into which microbeads can be self-assembled for transfer printing.

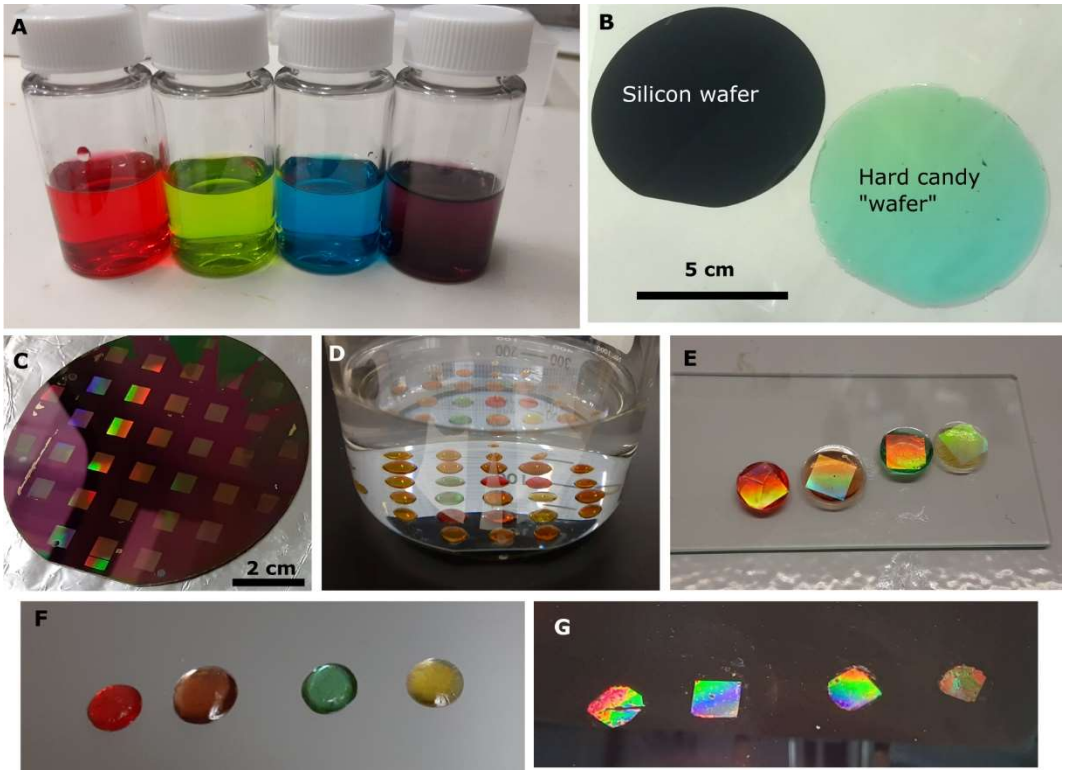

Fig. S12.

Reflow transfer using regular store-bought candy. (**A**) Sugar-water solutions created by dissolving differently flavored (and colored) hard candies with water 1:1 (in this case, different individual Jolly Ranchers in each vial, but any hard candy will do). (**B**) Example of a hard candy reformed into a thin 76 mm (3-inch) hard candy "wafer", by pouring sugar mixture from the blue vial in (A) over the silicon wafer shown alongside, evaporatively drying it, and then removing it from the wafer. (**C**) Arrays of 1-μm disks, to be transferred using the candy, prepared on top of a sacrificial photoresist layer on a silicon wafer. (**D**) The silicon wafer from (C) with drops of differently colored hard candy solution from the vials in (A) placed over the disk arrays, is shown submerged in a beaker of acetone used to dissolve the sacrificial photoresist layer. (Sugar does not dissolve in acetone). (**E**) Hard candy drops removed the silicon wafer and flipped upside down to show the now attached disk arrays on the undersides. (**F**) Same drops as in (E) flipped back over and placed on another silicon wafer for pattern transfer. (**G**) Transfer printed disk arrays after the hard candy drops seen in (F) are dissolved away in water. Diffraction colors show that even regular hard candy can accurately transfer micropatterns from one substrate to another.

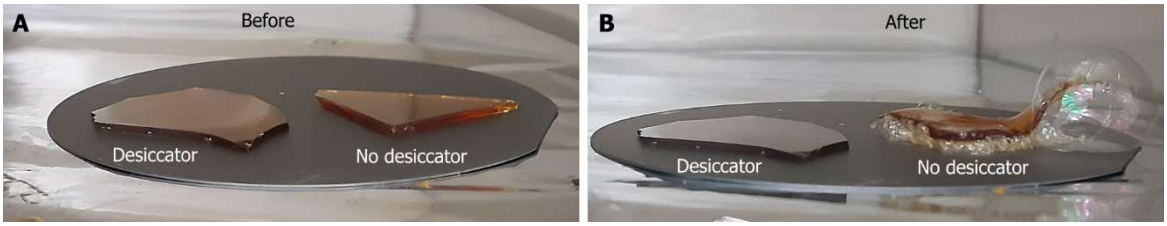

Fig. S13.

Water absorption impact on vapor pressures. (**A**) and (**B**), show photographs of two pieces of the same hardened sugar mixture (broken off of one larger piece) before and after heating together in a vacuum oven, respectively. The piece on the left was stored in a desiccator; the piece on the right was not. Water absorbed from background humidity lowers the T_g and increases the vapor pressure of the piece on the right, leading to bubbling, and rendering it unusable for any vacuum-based pattern transfer. By contrast, there is no bubbling of the left-hand piece.

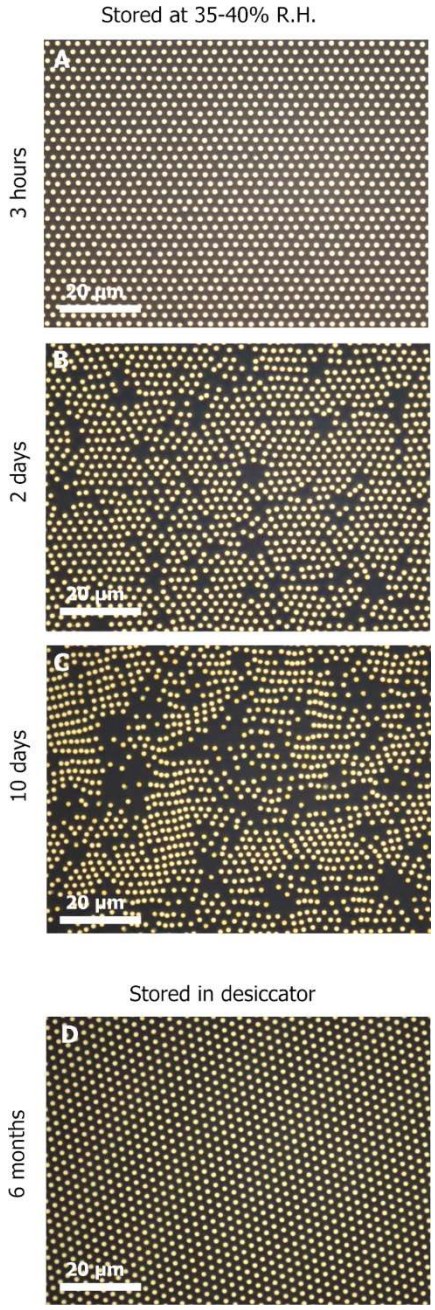

Fig. S14.

Pattern stability over time. (**A**), (**B**), and (**C**), optical micrographs of the same piece of hardened sugar with attached array of 1-µm disks after being stored in typical laboratory environment with 35-40% relative humidity (RH) for 3 hours, 2 days, and 10 days, respectively. Water absorbed from background humidity softens the sugar layer and the embedded disk array pattern reveals how this water uptake microscopically deforms the surface. By contrast (**D**) shows the same material after being stored in a desiccator for 6 months. Keeping the sugar dry maintains it in a stable glassy state that yields no observable deformation down to at least the sub-micron scale visible here. Transfer patterns can thus be stored attached to the transfer sugar carrier for extended periods if needed.

Movie S1.

Reflow patterning over the tip of a pin. The reflow transfer process is demonstrated using the extreme case of a transfer layer of sugar positioned over the sharp tip of a pin using two side supports (because the sugar cannot itself balance directly on the pin tip) and gradually heated. Video shows a timelapse (1 frame every 3 seconds) of the sugar softening and reflowing to transfer print the attached patterns around the pin tip (as in Fig. 1E).

Movie S2.

Stretchable diffraction grating with transfer patterned elastomer. A laser pointer beam is diffracted through an array of 1-μm disks transfer printed onto a flexible, transparent piece of polydimethylsiloxane (PDMS) (see fig. S8). As the PDMS is stretched and released the spacings between the disks comprising the transfer printed array changes, altering the resulting diffraction angles and observed diffraction pattern along the stretching axis.

Movie S3.

Continuous transfer patterning around all sides of a cube. An animated sequence of scanning electron micrographs taken at incremental angles around a transfer printed 50-μm cube, showing continuity of the transfer patterning around all sides.

Movie S4.

Magnetic manipulation of transfer printed milkweed floss fiber. An individual vertically standing milkweed seed floss fiber transfer printed with 1-μm diameter magnetic disks (Fig. 3D) reacts as a magnet is moved near to it and withdrawn.